

Large Intelligent Surfaces With Discrete Set of Phase-Shifts Communicating Through Double-Rayleigh Fading Channels

Felipe A. P. de Figueiredo, Michelle S. P. Facina, Ricardo C. Ferreira, and Gustavo Fraidenraich

Abstract—It is known that the Central Limit Theorem (CLT) is not always the most appropriate tool for deriving closed-form expressions. We evaluate a Single-Input Single-Output (SISO) system performance in which the Large Intelligent Surface (LIS) acts as a scatterer. The direct link between the transmitting and receiving devices is negligible. Quantization phase errors are considered since the high precision configuration of the reflection phases is not always feasible. We derive exact closed-form expressions for the spectral efficiencies, outage probabilities, and average symbol error rate (SER) of different modulations. We assume a more comprehensive scenario in which b bits are dedicated to the LIS elements' phase adjustment. From Monte Carlo simulations, we prove the excellent accuracy of our approach and investigate the behavior of power scaling law and power required to reach a specific capacity, depending on the number of reflecting elements. We show that the LIS with approximately fifty elements and four dedicated bits for phase quantization outperforms the conventional system performance without LIS.

Index Terms—LIS, outage probability, quantization phase errors, spectral efficiency, symbol error rate.

I. INTRODUCTION

There are no doubts that there are quantization errors. After all, they are inevitable when using the analog-to-digital converter (ADC). The famous converters bridge the analog world with the digital world. And the lower its resolution, the more distortions it can cause to the process. So, what we have left is to learn to deal with them. For mature systems like MIMO, for example, there are numerous solutions proposed to mitigate quantization errors.

Since the rounding quantization introduces error in the signal estimate stage, Hou et al. [1] propose a quantization error reduction scheme for detection based on orthogonal lattices. On the other hand, Kotera et al. [2] proves that an efficient nonlinear (Viterbi) as the equalization scheme can estimate both inter-symbol interference in multi-path channel and quantization error in ADC and improve the bit error rate (BER) performance.

But for Large Intelligent Surfaces (LIS) assisted systems, little is known. Also called Reconfigurable Intelligent Surfaces (RIS), this technology is a strong candidate to integrate the sixth generation (6G) of cellular networks. It consists of many electromagnetic elements act individually as scatterers and are capable of jointly reflecting the incident signals for the destination in the desired direction [3]. Among its advantages, we can mention the ideally passive nature that does not require any dedicated energy source. By not amplifying the signal,

LIS provides an inherently full-duplex transmission without introducing noise, unlike relays. Besides, it is easily installed onto facades of buildings or walls of rooms thanks to the lightweight and conformal geometry. Due to this smart adjust of the phase shifts, the reflected signals can add coherently or destructively at the receiver. The first strategy improves the received signal power, while the second one avoids interference of unwanted signals or receivers and increases the security of the communication system [4].

Taking advantage of LIS-assisted systems' low power consumption, [5] jointly optimize the transmit beamforming at the BS and the phase shifts at the IRS. From derived lower bounds of the transmit power concerning the number of antennas at the BS, the number of LIS elements, and the number of mobile users, they show that the transmit power at the BS is significantly lower than that of the communication systems without LIS.

Although some studies optimize the reflection coefficients (amplitude and phase) of each LIS element [6], the reflection phases' high precision configuration is unfeasible since the number of bits is limited. As a consequence, phase quantization errors arise. Before proposing techniques to reduce them, we first need to know them and estimate their effects as closely as possible to reality.

Badiu et al. do a preliminary analysis based on a limited number of reflectors and conclude that the performance measured from the error probability is robust against the phase errors [7]. Samith et al. [8] also consider a practical phase-shift model, but to maximize the achievable rate through the joint optimization of the transmit beamforming and the LIS reflect beamforming.

On the other hand, Han et al. [9] propose an optimal phase shift design that achieves approximately the ergodic capacity and ensures that a quantizer with two bits is sufficient for a capacity degradation below 1 bit/s/Hz.

As can be seen, there are many works in the literature about the optimization of LIS-assisted systems. We deviated a little from this idea and looked for more precise mathematical models in the face of possible scenarios.

In our previous work [10], we have used the Central Limit Theorem (CLT) to derive the bit error rate when there are phase estimation errors. However, it is known that the CLT is inaccurate when the number of elements in LIS is small, and the approximation error can be significant in the high Signal-to-Noise ratio (SNR) regime.

This time, we do an in-depth investigation of LIS-assisted

Single-Input Single-Output (SISO) systems when there are quantization errors. Considering channels between source and destination characterized as the double (cascaded) Rayleigh fading distributions [11]–[14], we derive exact closed-form expressions for the spectral efficiencies, outage probabilities, and average symbol error rate (SER). Our analysis also extends to power scaling law and the power required to achieve specific capacity. Based on our excellent accuracy approach, we evaluate the system performance as the number of bits and reflectors increases. We conclude that the LIS with approximately fifty elements and four dedicated bits for phase quantization outperforms the conventional system performance without LIS. To the best of our knowledge, no similar results have been found in the literature.

Wang et al. [15] also consider a SISO LIS-assisted system and derive exact expressions for outage probability and diversity order without employing a CLT approach. However, they assume that each element of LIS has only a one-bit phase shifter. We propose expressions for a more comprehensive scenario in which more bits are dedicated to the phase adjustment of the LIS elements.

The remainder of this paper is organized as follows: Section II presents the adopted model and the preliminary assumptions. In Section III, we derive exact closed-form expressions for some important performance parameters and evaluate the quantization error effects. Section IV shows our setup and the results obtained from it. Finally, Section V summarises the main conclusions.

Notations: Scalars are denoted by italic letters while vectors and matrices, by bold-face lower-case and uppercase letters, respectively. For a complex-valued vector \mathbf{x} , $|\mathbf{x}|$ denotes its Euclidean norm and $\text{diag}(\mathbf{x})$ represents the diagonal matrix. The distribution of a circularly symmetric complex Gaussian (CSCG) random vector with mean μ and covariance Ξ is denoted by $\mathcal{CN}(\mu, \Xi)$; and \sim stands for “distributed as”. For any general vector \mathbf{x} , x_i denote its i th element while \mathbb{E} is the statistical expectation. Finally, $\Pr(\cdot)$ represents the probability of a specific event occurring.

II. SYSTEM MODEL

The system model of the adopted LIS-assisted communications scheme is shown in Fig. 1, where g_n and h_n represent the fading channels between the single-antenna source (S) and the n th antenna element of the LIS, and the n th antenna element of the LIS and the single-antenna destination (D), respectively. Here we assume Rayleigh fading channels, *i.e.*, $g_n \sim \mathcal{CN}(0, \beta_g)$ and $h_n \sim \mathcal{CN}(0, \beta_h)$. The parameters β_g and β_h model the shadow and geometric attenuation fading, (*i.e.*, the large-scale fading coefficients), which are assumed to be independent over the elements of LIS and change very slowly over time, being constant over several coherence-time intervals [16]. This is a reasonable assumption since the distance between devices and LIS is much larger than the distance between the LIS’ elements. In this far-field regime [3], the intelligent surface is better modeled as a scatterer and the scaling law that governs the intensity of its electric field is a function of the distances’ product, as proved in [17] and shown later.

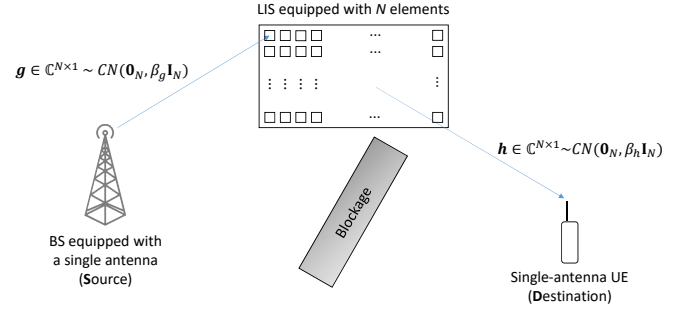


Figure 1. System Model.

We assume that the LIS is a reflect-array composed of N simple and re-configurable reflector elements connected to a controller. Additionally, we assume that the phase-shifts produced by the channels are estimated perfectly. However, the desired phases can not be accurately generated by the LIS once it has a discrete set of phases. Practical LISs have a limited number of phase shifts, *i.e.*, a discrete set of phase-shifts constrained by the number of quantization bits (also known as phase resolution) of the LIS. The number of quantization bits is denoted by b . Therefore, the set of phase shifts produced by each one of the elements of the LIS is defined as

$$\phi_n = \left\{ 0, \frac{2\pi}{2^b}, \frac{4\pi}{2^b}, \dots, \frac{2\pi(2^b - 1)}{2^b} \right\}. \quad (1)$$

Therefore, we model the deviation from the correct/ideal phase-shift as a phase-noise, δ_n , which is uniformly distributed in the range $[-\pi/Q, \pi/Q]$, where $Q = 2^b$ is the number of discrete phases the LIS can generate [18] dictated by the hardware complexity and power consumption of LIS.

III. INTELLIGENT TRANSMISSION THROUGH LIS

In slowly varying flat fading channels, the signal received at the destination after being reflected through a LIS composed of N passive elements can be written as

$$y = \sqrt{\rho} \left[\sum_{n=1}^N g_n e^{-j\phi_n} h_n \right] s + w, \quad (2)$$

where ρ is the average SNR, ϕ_n is the adjustable phase-shift produced by the n th LIS reflector, s is the modulation data symbol with zero mean, $\mathbb{E}[|s|^2] = 1$, and $w \sim \mathcal{CN}(0, 1)$ is the additive white Gaussian noise (AWGN) term.

Then, (4) can be re-written in the matrix-form as

$$y = \sqrt{\rho} \mathbf{h}^T \Phi \mathbf{g} s + w, \quad (3)$$

where $\mathbf{g} = [g_1, \dots, g_N]^T$ and $\mathbf{h} = [h_1, \dots, h_N]^T$ are the channel coefficient vectors between the BS and the RIS and between the RIS and the terminal, respectively, while $\Phi = \text{diag}([e^{-j\phi_1}, \dots, e^{-j\phi_N}])$ is the diagonal matrix containing the phase-shifts applied by the elements of the LIS.

It can be noticed that (3) is similar to the equation of conventional MIMO systems employing precoding/beamforming for transmission. However, differently from those systems, where precoding/beamforming is carried out at the transmitter

side, here it is carried out over the transmission medium (*i.e.*, the environment) [19].

The complex channels can be written in polar representation (*i.e.*, with magnitude and phase) as $h_n = \alpha_n e^{j\theta_n}$ and $g_n = \xi_n e^{j\psi_n}$, therefore, (4) can be re-written as

$$\begin{aligned} y &= \sqrt{\rho} \left[\sum_{n=1}^N \alpha_n \xi_n e^{j(\theta_n + \psi_n - \phi_n)} \right] s + w \\ &= \sqrt{\rho} \left[\sum_{n=1}^N \alpha_n \xi_n e^{j\delta_n} \right] s + w, \end{aligned} \quad (4)$$

where the second line is obtained from the assumption that the LIS only generates discrete phases and consequently, there is a phase-noise, $\delta_n = \theta_n + \psi_n - \phi_n$.

Considering the phase-noise, then the instantaneous SNR at the destination is given by

$$\gamma = \rho \left| \sum_{n=1}^N \alpha_n \xi_n e^{j\delta_n} \right|^2. \quad (5)$$

Note that the instantaneous SNR is maximized when $\delta_n = 0$, *i.e.*, the channels are perfectly estimated, and the LIS can accurately generate the phases induced by the channels (meaning that $Q \rightarrow \infty$) [20].

Lemma 1. *From empirical comparisons between the normalised histogram of the random variable given by*

$$r = \sqrt{\rho} \left| \sum_{n=1}^N \alpha_n \xi_n e^{j\delta_n} \right| = \sqrt{\rho} \left| \sum_{n=1}^N |g_n| |h_n| e^{j\delta_n} \right|, \quad (6)$$

and the theoretical PDF of a Gamma random variable, it is possible to say that the PDF of r can be accurately approximated by the Gamma PDF with shape and scale parameters given by κ and θ , respectively as

$$\kappa = \frac{-(\mathbb{E}[\gamma^2] - 5\mathbb{E}[\gamma]^2) + \sqrt{(\mathbb{E}[\gamma^2])^2 - 34\mathbb{E}[\gamma^2]\mathbb{E}[\gamma]^2 + 49\mathbb{E}[\gamma]^4}}{2(\mathbb{E}[\gamma^2] - \mathbb{E}[\gamma]^2)} > 0, \quad (7)$$

$$\theta = \sqrt{\frac{-\sqrt{(\mathbb{E}[\gamma^2])^2 + 14\mathbb{E}[\gamma^2]\mathbb{E}[\gamma]^2 + \mathbb{E}[\gamma]^4} + 2\mathbb{E}[\gamma^2] + 2\mathbb{E}[\gamma]^2}}{6\mathbb{E}[\gamma]}} > 0, \quad (8)$$

where $\mathbb{E}[\gamma]$ and $\mathbb{E}[\gamma^2]$ are given by (11) and (12), respectively.

Some examples of this comparison are shown in Section IV. The parameters κ and θ are found following the rationale presented in Appendix A. Therefore, the PDF of γ can be found following the standard transformation of random variables, $\gamma = r^2$, and is defined as

$$f_\gamma(\gamma) = \frac{1}{2\Gamma(\kappa)\theta^\kappa} \gamma^{\left(\frac{\kappa-2}{2}\right)} e^{-\frac{\sqrt{\gamma}}{\theta}}, \gamma \geq 0. \quad (9)$$

In its turn, the cumulative distribution function (CDF) of the SNR random variable, γ , is defined as

$$F_\gamma(\gamma) = \int_0^\gamma f_\gamma(x) dx = 1 - \frac{\Gamma\left(\kappa, \frac{\sqrt{\gamma}}{\theta}\right)}{\Gamma(\kappa)}, \gamma \geq 0, \quad (10)$$

where $\Gamma(\cdot)$ is the Euler gamma function while $\Gamma(\cdot, \cdot)$ is the upper incomplete gamma function. The integral result is obtained by directly applying (Eq. 2.33.10, [21]).

Remark 1. *When $Q \rightarrow \infty$, *i.e.*, the LIS is able to generate any phase-shift, the phase-noise is zero, $\delta_n = 0, \forall n$, and consequently, (11) and (12) can be simplified to (13) and (14), respectively, and whose derivations are presented in Appendix B.*

A. Exact Ergodic Spectral Efficiency

The ergodic spectral efficiency of the LIS-assisted system is defined as

$$\begin{aligned} C &= \mathbb{E}[\log_2(1 + \gamma)] \\ &= \int_0^\infty \log_2(1 + \gamma) f_\gamma(\gamma) d\gamma. \end{aligned} \quad (15)$$

Solving (15) through an integral solver [22], we find the exact closed-form expression for the ergodic capacity given by (16), where ${}_pF_q(a_1, \dots, a_p; b_1, \dots, b_q; z)$ is the generalized hypergeometric function [23] and $\Psi^{(n)}(z)$ is the n th derivative of the digamma function, also known as the polygamma function [24].

Remark 2. *In high SNR regime, the ergodic spectral efficiency in (16) can be approximated as in (17).*

Remark 3. *When $\rho \rightarrow \infty$, then (16) becomes (18).*

$$\lim_{\rho \rightarrow \infty} C = \frac{4 \log(\theta)}{\log(4)}. \quad (18)$$

The proofs for Remarks 2 and 3 are presented in Appendices C and D, respectively.

Remark 4. *In high SNR and N regimes, the ergodic spectral efficiency can be approximated as*

$$C_{\text{high-SNR}, N} \approx \frac{2}{\theta^2(\kappa - 1)(\kappa - 2) \log(4)} + \frac{4(\log(\theta) + \psi^{(0)}(\kappa))}{\log(4)}. \quad (19)$$

The proof for Remark 4 is presented in Appendix E.

Other alternative to find the expectation in (15) is using the PDF of the random variable given by $C_{\text{inst.}} = \log_2(1 + \gamma)$, *i.e.*, the instantaneous spectral efficiency, which can be found after applying standard transformation of random variables to (9) giving rise to

$$f_{C_{\text{inst.}}}(c) = \frac{\log(2)}{\Gamma(\kappa)\theta^\kappa} 2^{c-1} (2^c - 1)^{\left(\frac{\kappa-2}{2}\right)} e^{-\frac{\sqrt{2^c-1}}{\theta}}, c \geq 0. \quad (20)$$

Then, the CDF of the instantaneous spectral capacity random variable is expressed by

$$F_{C_{\text{inst.}}}(c) = \int_0^c f_{C_{\text{inst.}}}(x) dx = 1 - \frac{\Gamma\left(\kappa, \frac{\sqrt{2^c-1}}{\theta}\right)}{\Gamma(\kappa)}, \quad (21)$$

whose integral is also found by directly applying (Eq. 2.33.10, [21]).

$$\mathbb{E}[\gamma] = \mathbb{E}[r^2] = \rho\beta_g\beta_h\mathcal{A}_1 = \rho\beta_g\beta_h N \left[1 + \frac{1}{16}(N-1)Q^2 \sin^2\left(\frac{\pi}{Q}\right) \right]. \quad (11)$$

$$\begin{aligned} \mathbb{E}[\gamma^2] &= \mathbb{E}[r^4] = (\rho\beta_g\beta_h)^2 \mathcal{A}_2 \\ &= (\rho\beta_g\beta_h)^2 \frac{N}{256} \left\{ 512(N+1) + \frac{32(N-1)Q^2}{\pi^2} + \frac{(N-1)Q^2 \left[\pi \sin^2\left(\frac{\pi}{Q}\right) \left((N-2)Q \left(\pi(N-3)Q \sin^2\left(\frac{\pi}{Q}\right) + 16 \sin\left(\frac{2\pi}{Q}\right) \right) + 16\pi(4N+1) - 32 \cos\left(\frac{4\pi}{Q}\right) \right) \right]}{\pi^2} \right\}. \end{aligned} \quad (12)$$

$$\lim_{Q \rightarrow \infty} \mathbb{E}[\gamma] = N\rho\beta_g\beta_h \left[1 + \frac{(N-1)\pi^2}{16} \right]. \quad (13)$$

$$\lim_{Q \rightarrow \infty} \mathbb{E}[\gamma^2] = \frac{N\rho^2(\beta_g\beta_h)^2}{256} [256 + 768N + \pi^4(N-3)(N-2)(N-1) + 48\pi^2(2N-1)(N-1)]. \quad (14)$$

$$\begin{aligned} C &= \frac{2 {}_2F_3\left(1, 1; 2, \frac{3}{2} - \frac{\kappa}{2}, 2 - \frac{\kappa}{2}; -\frac{1}{4\theta^2}\right) - 2\pi \sec\left(\frac{\pi\kappa}{2}\right) {}_1F_2\left(\frac{\kappa}{2} + \frac{1}{2}; \frac{3}{2}, \frac{\kappa}{2} + \frac{3}{2}; -\frac{1}{4\theta^2}\right)}{\theta^2(\kappa-1)(\kappa-2)\log(4)} - \frac{2\pi \sec\left(\frac{\pi\kappa}{2}\right) {}_1F_2\left(\frac{\kappa}{2} + \frac{1}{2}; \frac{3}{2}, \frac{\kappa}{2} + \frac{3}{2}; -\frac{1}{4\theta^2}\right)}{(\kappa+1)\theta^{\kappa+1}\Gamma(\kappa)\log(4)} \\ &+ \frac{2\pi \csc\left(\frac{\pi\kappa}{2}\right) {}_1F_2\left(\frac{\kappa}{2}; \frac{1}{2}, \frac{\kappa}{2} + 1; -\frac{1}{4\theta^2}\right)}{\kappa\theta^\kappa\Gamma(\kappa)\log(4)} + \frac{4(\log(\theta) + \psi^{(0)}(\kappa))}{\log(4)}. \end{aligned} \quad (16)$$

$$C_{\text{high-SNR}} \approx \frac{2}{\theta^2(\kappa-1)(\kappa-2)\log(4)} - \frac{2\pi \sec\left(\frac{\pi\kappa}{2}\right)}{(\kappa+1)\theta^{\kappa+1}\Gamma(\kappa)\log(4)} + \frac{2\pi \csc\left(\frac{\pi\kappa}{2}\right)}{\kappa\theta^\kappa\Gamma(\kappa)\log(4)} + \frac{4(\log(\theta) + \psi^{(0)}(\kappa))}{\log(4)}. \quad (17)$$

$$C \leq C_{\text{upper}} = \log_2 \left(1 + N\rho\beta_g\beta_h \left[1 + \frac{1}{16}(N-1)Q^2 \sin^2\left(\frac{\pi}{Q}\right) \right] \right). \quad (22)$$

$$\begin{aligned} C_{\text{upper}}^{\max} &= \lim_{Q \rightarrow \infty} C_{\text{upper}} \\ &= \lim_{Q \rightarrow \infty} \log_2 \left(1 + N\rho\beta_g\beta_h \left[1 + \frac{1}{16}(N-1)Q^2 \sin^2\left(\frac{\pi}{Q}\right) \right] \right) \\ &= \log_2 \left(1 + N\rho\beta_g\beta_h \left[1 + \frac{(N-1)\pi^2}{16} \right] \right). \end{aligned} \quad (23)$$

$$\begin{aligned} C &\geq C_{\text{lower}} \approx \log_2 \left(1 + \frac{\mathbb{E}[\gamma]^3}{\mathbb{E}[\gamma^2]} \right) \\ &= \log_2 \left(1 + \frac{256N^2\rho\beta_g\beta_h \left(\frac{1}{16}(N-1)Q^2 \sin^2\left(\frac{\pi}{Q}\right) + 1 \right)^3}{\frac{32(N-1)Q^2}{\pi^2} + \frac{(N-1)Q^2 \left(\pi \sin^2\left(\frac{\pi}{Q}\right) \left((N-2)Q \left(\pi(N-3)Q \sin^2\left(\frac{\pi}{Q}\right) + 16 \sin\left(\frac{2\pi}{Q}\right) \right) + 16\pi(4N+1) - 32 \cos\left(\frac{4\pi}{Q}\right) \right) \right)}{\pi^2} + 512(N+1)} \right). \end{aligned} \quad (24)$$

$$\begin{aligned} C_{\text{lower}}^{\max} &= \lim_{Q \rightarrow \infty} C_{\text{lower}} \\ &= \log_2 \left(1 + \frac{N^2\rho\beta_g\beta_h (\pi^2(N-1) + 16)^3}{16((N-1)(\pi^4(N^2 - 5N + 6) + 48\pi^2(2N-1) + 256) + 512(N+1))} \right). \end{aligned} \quad (25)$$

B. Upper and Lower-bounds for the Ergodic Spectral Efficiency

As it can be seen, (16) is quite complex. Therefore, here we aim at finding simpler but yet tight bounds for the ergodic spectral efficiency of the LIS-assisted system. According to Jensen's inequality [16], it holds that

$$\mathbb{E}[\log_2(1 + \gamma)] \leq \log_2(1 + \mathbb{E}[\gamma]). \quad (26)$$

Then, by using $\mathbb{E}[\gamma]$ given by (11), a possible upper-bound for the ergodic capacity of the LIS-assisted system can be

given by (22). As it is tight for high SNR scenarios, it can be assumed as a good approximation.

On the other hand, again according to Jensen's inequality [16], it holds that

$$\mathbb{E}[\log_2(1 + \gamma)] \geq \log_2 \left(1 + \left[\mathbb{E} \left[\frac{1}{\gamma} \right] \right]^{-1} \right). \quad (27)$$

Consequently, by using a tight approximation of $\mathbb{E}[1/\gamma]$ (see Appendix F), a lower-bound for the ergodic capacity of the LIS-assisted system can be derived and given as (24).

Like the SNR, the spectral efficiency is also maximized when $Q \rightarrow \infty$, meaning that the LIS has infinite phase-shift precision and can generate any phase-shift. In this case, the maximum ergodic spectral efficiency with the upper and lower bounds are given by (23) and (25), respectively.

C. Impact of Bit Quantization in the Spectral Efficiency

In practical communication systems, the set of phase-shifts is limited by the number of quantization bits of the LIS, influencing the achieved spectral efficiency directly. Therefore, in this section, we propose a criterion for selecting the number of quantization levels $Q = 2^b$ so that the ergodic spectral efficiency is optimized up to a specific spectral degradation in bits/s/Hz. In order to quantify this degradation, we define the error ϵ brought about by a limited number of phase-shifts as

$$C_{\text{upper}}^{\text{max.}} - C_{\text{upper}} \leq \epsilon. \quad (28)$$

Remark 5. From (28), we see that when the number of LIS elements tends to ∞ , then the ergodic spectral efficiency degradation, ϵ , becomes

$$\lim_{N \rightarrow \infty} \epsilon = \log_2 \left(\frac{\pi^2}{Q^2 \sin^2(\pi/Q)} \right) \text{ bits/s/Hz}. \quad (29)$$

Remark 6. From (28), we see that when $\rho \rightarrow \infty$, then the ergodic spectral efficiency degradation, ϵ , is given by

$$\lim_{\rho \rightarrow \infty} \epsilon = \log_2 \left(\frac{16 + (N-1)\pi^2}{16 + (N-1)Q^2 \sin^2(\pi/Q)} \right) \text{ bits/s/Hz}. \quad (30)$$

Proposition 1. In order to guarantee an suitable ergodic spectral efficiency degradation of ϵ bits/s/Hz compared to a LIS with full-resolution phase-shift, the number of quantization levels, Q , of the LIS should satisfy

$$Q \sin(\pi/Q) \geq \sqrt{\frac{16(2^{-\epsilon} - 1)}{N\rho\beta_g\beta_h(N-1)} + \frac{16(2^{-\epsilon} - 1)}{N-1} + \pi^2 2^{-\epsilon}}. \quad (31)$$

Remark 7. From (31), we see that when $N \rightarrow \infty$, the number of quantization levels, Q , should satisfy

$$\lim_{N \rightarrow \infty} Q \sin(\pi/Q) \geq \sqrt{2^{-\epsilon}} \pi. \quad (32)$$

Remark 8. From (31) we see that when $\epsilon \rightarrow \infty$, then the number of quantization levels, Q , should satisfy

$$\lim_{\epsilon \rightarrow \infty} Q \sin(\pi/Q) \leq \pi. \quad (33)$$

After analysing Remark 8, we notice that the first term in (33) is equal to π only when $Q \rightarrow \infty$. Therefore, in order to have no degradation at all, an infinite number of quantization levels is necessary, which demonstrates the correctness of Remark 8.

Summing up, these results can be used to select the precision necessary for a LIS-assisted system to achieve a pre-defined and acceptable degradation in its ergodic spectral efficiency.

D. Outage Probability

Based on the knowledge of the approximate PDF of the instantaneous spectral efficiency given by (20), it is possible to find its cumulative density function (CDF) and derive analytical expressions for the outage probability. The outage probability is defined as the probability that the achieved instantaneous spectral efficiency falls below a given threshold C_{out} and can be written as

$$\begin{aligned} P_{\text{out.}} &= \Pr\{C_{\text{inst.}} < C_{\text{out.}}\} \\ &= \int_0^{C_{\text{out.}}} f_{C_{\text{inst.}}}(x) dx \\ &= 1 - \frac{\Gamma\left(\kappa, \frac{\sqrt{2C_{\text{out.}}-1}}{\theta}\right)}{\Gamma(\kappa)}, \end{aligned} \quad (34)$$

whose proof is provided in Appendix G.

Besides that way, the outage probability can also be defined with regard to the instantaneous SNR. In this case, it is the probability that the instantaneous SNR falls below a given SNR threshold γ_{out} . So, the outage probability is given by

$$\begin{aligned} P_{\text{out.}} &= \Pr\{\gamma < \gamma_{\text{out.}}\} \\ &= \int_0^{\gamma_{\text{out.}}} f_{\gamma}(x) dx \\ &= \frac{1}{\theta^{\kappa/2}} \left[1 - \frac{\Gamma\left(\kappa, \frac{\sqrt{\gamma_{\text{out.}}}}{\theta}\right)}{\Gamma(\kappa)} \right], \end{aligned} \quad (35)$$

and found by using (92) in Appendix G. It can also be expressed as

$$P_{\text{out.}} = \frac{\gamma_{\text{out.}}^{\frac{\kappa}{2}}}{\kappa\theta^{\frac{3\kappa}{2}}} {}_1F_1\left(\kappa, \kappa + 1, -\frac{\sqrt{\gamma_{\text{out.}}}}{\theta}\right). \quad (36)$$

Remark 9. In high SNR regime, the outage probability can be approximated as

$$P_{\text{out.}}^{\text{high-SNR}} = \frac{\gamma_{\text{out.}}^{\frac{\kappa}{2}}}{\kappa\theta^{\frac{3\kappa}{2}}}. \quad (37)$$

The proofs of (36) and (37) are provided in Appendix H.

E. Average Symbol Error Rate

According to [25], the average Symbol Error Rate (SER) is defined as the expectation of conditional error probability, $P_{e|\gamma}$, given the distribution of the SNR, γ . For a wide variety of modulation schemes, $P_{e|\gamma}$ is defined as $P_{e|\gamma} = a\mathcal{Q}(\sqrt{b\gamma})$, where a and b are constant modulation dependent parameters and \mathcal{Q} is the Gaussian \mathcal{Q} -function defined as $\int_x^\infty e^{-t^2/2}/\sqrt{2\pi} dt$ [25]. Therefore, the average SER is derived as

$$\mathbb{E}\left[a\mathcal{Q}(\sqrt{b\gamma})\right] = a \int_0^\infty \mathcal{Q}(\sqrt{b\gamma}) f_{\gamma}(\gamma) d\gamma, \quad (38)$$

and can be analytically expressed by (40). The proof of (40) is provided in Appendix I.

Note that in (40), a and b are constants that depend on the modulation scheme. For instance, the average SER of the binary phase shift keying (BPSK) modulation is obtained when $a = 1$ and $b = 2$, while that for the M -ary Pulse Amplitude

Modulation (M -PAM), $a = 2(M-1)/M$ and $b = 6/(M^2-1)$. In the same way, $a = b = 2$ are applied for the average SER of the quadrature phase shift keying (QPSK) modulation. Finally, $a = 2$ and $b = 2 \sin^2(\pi/M)$ for M -ary phase shift keying (M-PSK) modulation, while $a = 4(1 - 1/\sqrt{M})$ and $b = 3/(M-1)$ for the average SER of the M -ary quadrature amplitude modulation (M-QAM), when $M > 4$.

Remark 10. *In high SNR regime, the average SER can be approximated as*

$$P_e^{\text{high-SNR}} \approx a 2^{-\frac{\kappa}{2}-1} b^{-\frac{\kappa}{2}} \theta^{-\kappa} \left(\frac{1}{\Gamma(\frac{\kappa}{2} + 1)} - \frac{\kappa}{\sqrt{2b\theta} \Gamma(\frac{\kappa+3}{2})} \right), \quad (39)$$

whose proof is provided in Appendix J.

After analyzing (39), it is possible to observe that the first term inside the parentheses is the dominant one. Otherwise, the average SER would be a negative number since a , b , and θ are values greater than zero. This direct insight results in the following remark.

Remark 11. *The average SER decreases when κ and/or b increases and when a and/or θ decreases.*

As shown in Section IV, this remark demonstrates that the average SER decreases as the transmission power, ρ , and/or the number of reflecting elements, N , increases. On the other hand, the average SER increases as the modulation order increases.

F. Diversity Order

The diversity order is a fundamental parameter of diversity-based systems. It measures the number of independent paths over which the data is received. The diversity order, D , is formally defined as the negative slope of the average SER versus the average SNR curve in a log-log scale, and calculated as by [26]

$$D = \lim_{\rho \rightarrow \infty} - \frac{\log P_e}{\log \rho}. \quad (41)$$

From the definition above, we can see that the diversity order is a high-SNR concept.

Remark 12. *The diversity order of the LIS-assisted system is obtained as*

$$D = \frac{5\mathcal{A}_1^2 + \sqrt{49\mathcal{A}_1^4 - 34\mathcal{A}_1^2\mathcal{A}_2 + \mathcal{A}_2^2} - \mathcal{A}_2}{4(\mathcal{A}_2 - \mathcal{A}_1^2)}. \quad (42)$$

The parameters and proof of (42) are detailed in Appendix K. From them, we realise that the diversity order increases as N .

Remark 13. *Despite both source and destination are equipped with a single antenna, the achievable diversity order grows with the number of LIS reflecting elements. It is worth noting that each reflecting element modifies the incident waves' phases to add at the destination coherently. A direct SISO path between source and destination would only allow for a unitary diversity order, once diversity gains can only be obtained by employing multiple antennas at transmission*

and/or receiving sides. However, a LIS employment provides a substantial diversity order to the communication system just by adding passive reflecting elements with adjustable phases to the system.

G. Power-scaling law

This subsection analyses the power-scaling law of the ergodic spectral efficiency regarding the number of reflecting elements in a LIS-assisted system in which $N \rightarrow \infty$.

If N grows without limit and we consider that the transmit power, ρ , can be scaled down with N^2 according $\rho = P/N^2$ and P is fixed, then (22) and (23) become, respectively

$$C_{\text{upper}} = \log_2 \left(1 + N \frac{P}{N^2} \beta_g \beta_h \left[1 + \frac{(N-1)Q^2 \sin^2\left(\frac{\pi}{Q}\right)}{16} \right] \right) \\ \rightarrow \frac{P \beta_g \beta_h Q^2 \sin^2\left(\frac{\pi}{Q}\right)}{16}, N \rightarrow \infty \quad (43)$$

and

$$C_{\text{upper}}^{\text{max.}} = \log_2 \left(1 + N \frac{P}{N^2} \beta_g \beta_h \left[1 + \frac{(N-1)\pi^2}{16} \right] \right) \\ \rightarrow \frac{P \beta_g \beta_h \pi^2}{16}, N \rightarrow \infty. \quad (44)$$

These results confirm that with many reflecting elements and perfect channel information, the transmit power can be reduced proportionally to $1/N^2$ without compromising the spectral efficiency.

Remark 14. *From (22) and (43), it is possible to see that if we decrease the transmit power proportionally to $1/N^\alpha$, with $\alpha > 2$, then the SNR goes to zero as $N \rightarrow \infty$. When $\alpha < 2$, the SNR grows without bound as $N \rightarrow \infty$. This means that $1/N^2$ (i.e., $\alpha = 2$) is the fastest rate at which we can decrease the transmit power and still maintain a fixed rate.*

The Remark 14 shows that as N grows without bound, the transmit power can be reduced proportionally to $1/N^2$. The transmit power reduction is significant mainly to power-constrained devices such as Internet of Things (IoT) devices [27, 28].

IV. SIMULATION RESULTS

This section presents some numerical results to validate the Monte Carlo simulations obtained from 10^6 realizations. The setup in Figure 2 shows the relative positions adopted. r_g and r_h are the distance between source and LIS, and between LIS and destination, respectively. Both of them are set to 25 m.

We assume that the large-scale fading coefficients are modeled as $\beta_h = z_h/(r_h)^\nu$ and $\beta_g = z_g/(r_g)^\nu$, in which z_h and z_g are log-normal random variables with standard deviation σ_{shadow} , while r_h is the distance between the source and the LIS and r_g is the distance between the LIS and the destination. ν is the path-loss exponent. For all simulation results, we adopt the typical suburban area parameters $\sigma_{\text{shadow}} = 8$ dB and $\nu = 3, 6, 7$.

Figure 3 presents some comparisons of the normalized histogram of the random variable given by the instantaneous

$$P_e = \mathbb{E} \left[aQ \left(\sqrt{b\gamma} \right) \right] = a2^{-\frac{\kappa}{2}-1} b^{-\frac{\kappa}{2}} \theta^{-\kappa} \left(\frac{{}_2F_2 \left(\frac{\kappa}{2} + \frac{1}{2}, \frac{\kappa}{2}; \frac{1}{2}, \frac{\kappa}{2} + 1; \frac{1}{2b\theta^2} \right)}{\Gamma \left(\frac{\kappa}{2} + 1 \right)} - \frac{\kappa {}_2F_2 \left(\frac{\kappa}{2} + \frac{1}{2}, \frac{\kappa}{2} + 1; \frac{3}{2}, \frac{\kappa}{2} + \frac{3}{2}; \frac{1}{2b\theta^2} \right)}{\sqrt{2b\theta} \Gamma \left(\frac{\kappa+3}{2} \right)} \right). \quad (40)$$

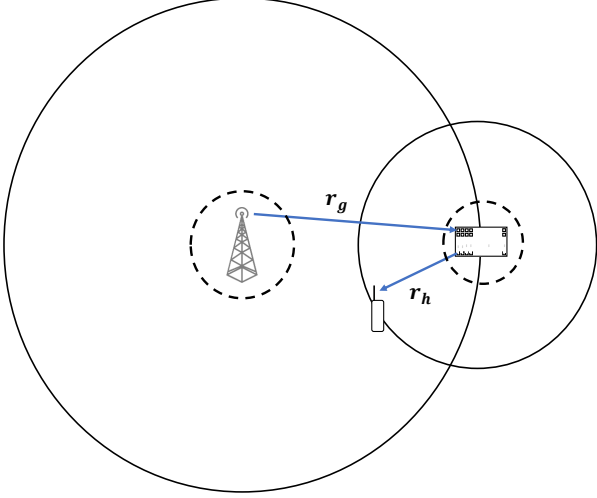


Figure 2. Adopted setup.

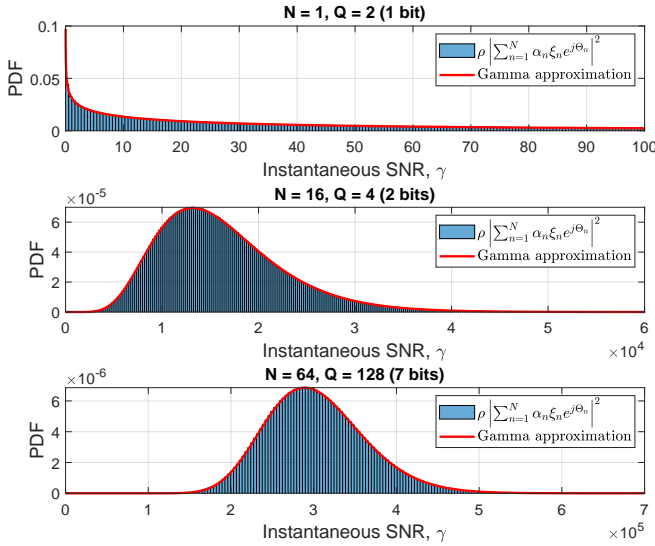


Figure 3. Comparison of the approximated PDF for the instantaneous sum-capacity.

SNR (see (5)) against the theoretical PDF given by (9). As can be noticed, even for a small number of reflecting elements and quantization bits, the approximation is quite tight.

Figure 4 shows the Kullback-Leibler Divergence [29] between the approximated SNR PDF and the real distribution of the SNR random variable over the variation of the number of quantization bits and for several values of LIS elements, N . In general, this is the most known technique to evaluate an approximation in statistics. As can be seen, from $b = 2$ bits, the divergence remains constant regardless of the number of elements. However, on the other hand, as the number of elements increases, the divergence decreases. These results

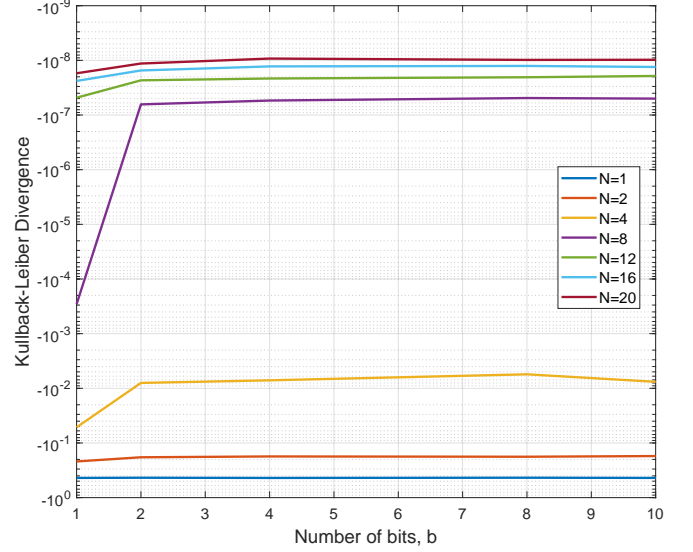


Figure 4. Kullback-Leibler divergence between the approximated SNR PDF and the real distribution.

show that only the number of LIS reflecting elements can take the approximated PDF closer to the real one and that the number of quantization bits has minimal impact on it. It is aligned to the theory since an inspection of (6) reveals that only the number of reflecting elements impact the summation in that equation.

From Figure 5 that show the spectral efficiency as a function of N for $b \in \{1, 4, 10\}$, we can see that the accuracy of the approximation becomes better not only as N increases but also when more bits are dedicated to quantization. For comparison, we also present the simulated capacity curve of the SISO system without LIS. When $b = 1$, LIS becomes advantageous for $N > 80$. Otherwise, When $b > 1$, a LIS with $N > 50$ is enough for its behavior to outperform that of the system without LIS.

We also verify performance degradation when b varies. As shown in Figure 6, the spectral efficiency decreases when b is small. This is evident, especially for $b = 1$ and $b = 2$. But the degradation tends to decrease as more reflective elements the LIS has. That is, for a LIS with many elements, a few bits are sufficient for quantization.

Regarding the distance between the source and the LIS, we compare the schemes' spectral efficiencies with $N = 25, 50, 100, 250, 500$. Figure 7 shows the results obtained for the worst case, when $b = 1$. We can see that the performance deteriorates as the distance increases. This phenomenon was expected since the LIS is composed of only passive elements and there is no direct path between the source and the user. However, as already mentioned, it improves when the number of elements on LIS increases.

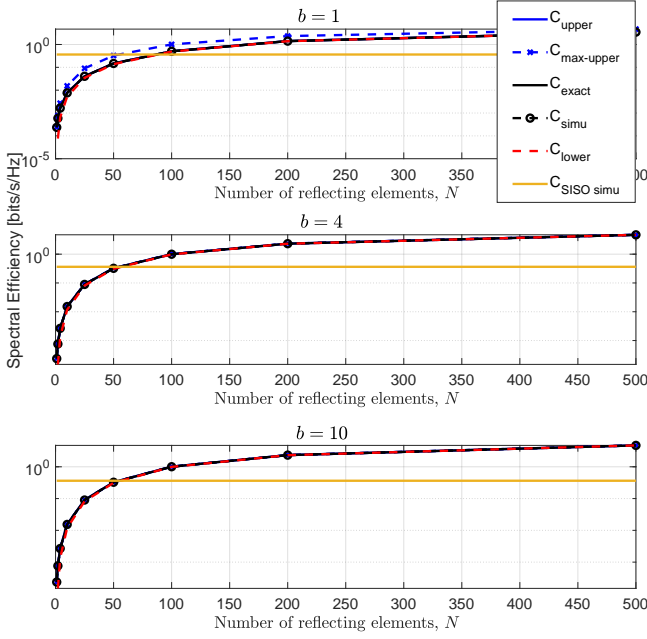


Figure 5. Spectral efficiency as a function of N for $b = 1$, $b = 4$ and $b = 10$.

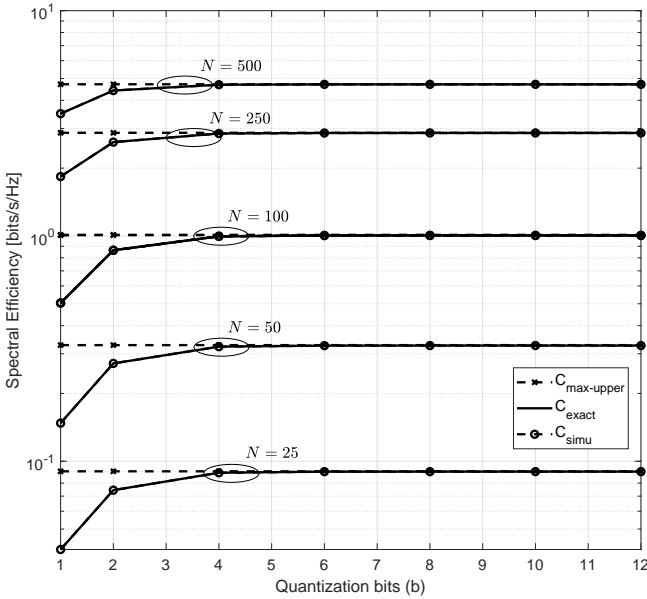


Figure 6. Spectral efficiency as a function of b for different values of N .

In its turn, Figure 8 shows how the spectral efficiency behaves as $\rho = P/N^\alpha$, with $\alpha = 3/2, 2, 5/2$. We consider $P = 100$ [dB] and $b \in \{1, 2, 4, 8, 10\}$. As expected and stated in Remark 14, for $\alpha \leq 2$ and increasing N , the capacity decreases or becomes constant no matter the number of antennas. However, when $\alpha > 2$, the capacity grows logarithmically fast with N when $N \rightarrow \infty$. These results confirm that the transmit power can be reduced proportionally to N . We can also see that, although the capacity increases with the number of quantization bits, the performances of $b = 4$, $b = 8$, and $b = 10$ are close.

Figure 9, we show the required transmit power by source needed to achieve fixed capacities of 1 and 2 bits/s/Hz,

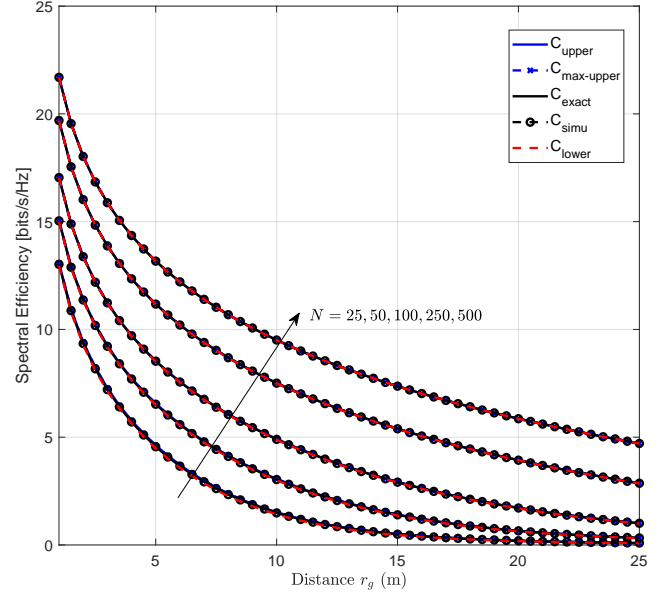


Figure 7. Spectral efficiency as a function of the distance between source and LIS, considering $b = 1$.

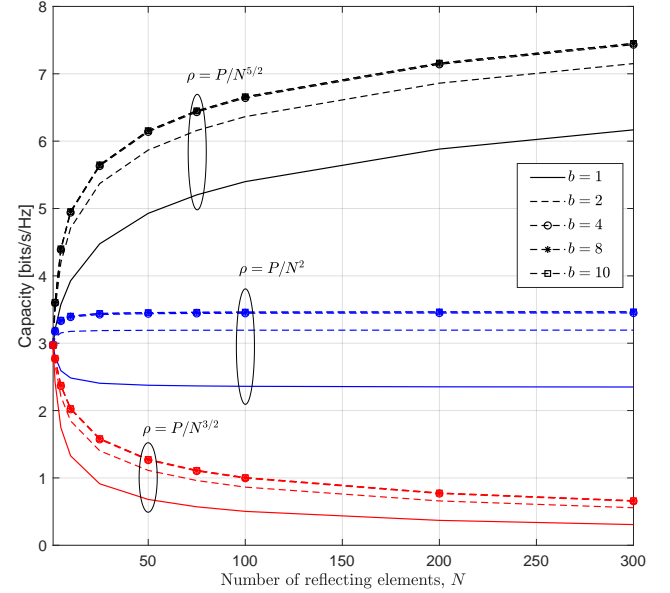


Figure 8. Power scaling law for different α values.

respectively represented by solid and dashed lines. As expected and predicted by Remark 14, the transmit power can be reduced by approximately 6 [dB] by doubling the number of LIS elements for both capacities. We can also confirm that, in general, the system LIS-assisted system outperforms the SISO system without LIS for approximately $N > 80$ regardless of the number of quantization bits.

Figure 10 compares the average SNR as a function of the transmitted power obtained from the simulations, (11), and the SISO system without LIS. We consider $\rho = 50$ dB, $N \in \{25, 100, 200\}$ and $b \in \{1, 4, 8\}$. As we can confirm, the relationship between the two parameters is linear. It is also worth mentioning that the LIS-assisted system outperforms the conventional the higher N . Moreover, the quantization bits'

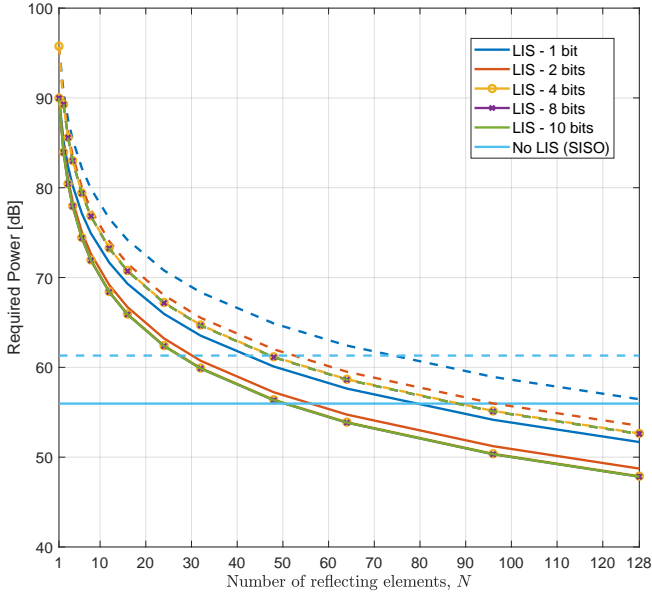


Figure 9. Required power for $C = 1$ bit/s/Hz (solid lines) and $C = 2$ bits/s/Hz (dashed lines).

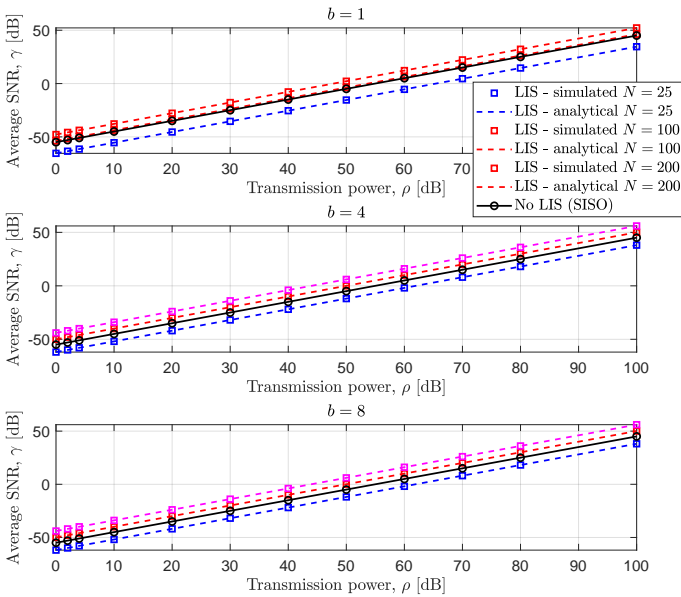


Figure 10. Average SNR in function of transmission power for $b = 1$, $b = 4$ and $b = 8$.

influence is not as significant, as long as $b > 1$.

Figure 11 shows the symbol error rate behavior for BPSK, QPSK, 16-QAM, and 64-QAM considering $N = 25$. As expected, the modulations present a decreasing level of robustness. The most important thing to note is the gap between the curves of 1, 2, and 4 bits. It gets to be almost 5dB when SNR is high. Although this gap exists, it is less pronounced when more bits are dedicated to phase quantization, and $b = 4$ is enough to guarantee a good performance.

For computational simplicity, in Figure 12, we represent the simulated and analytical outage probabilities only for $N = 100$. When considering different b values, it is possible to confirm the previous insight; $b = 4$ is enough for a good

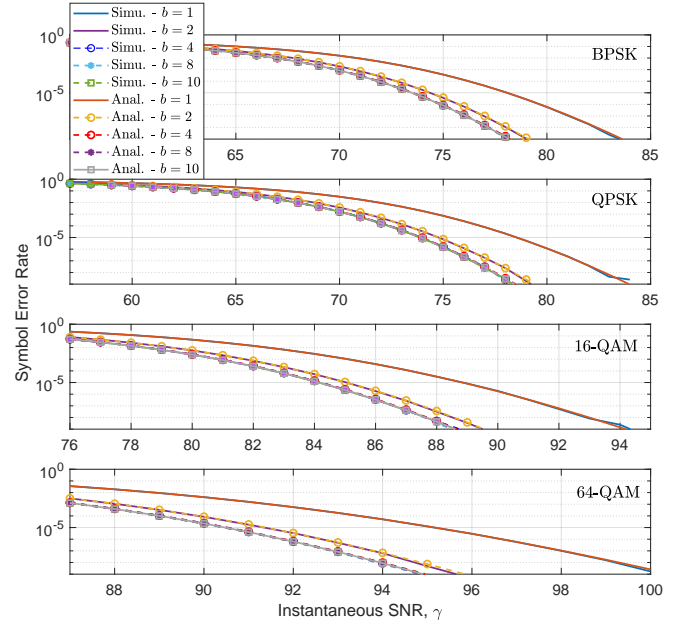


Figure 11. Symbol Error Rate for BPSK, QPSK, 16-QAM and 64-QAM modulations for $N = 25$.

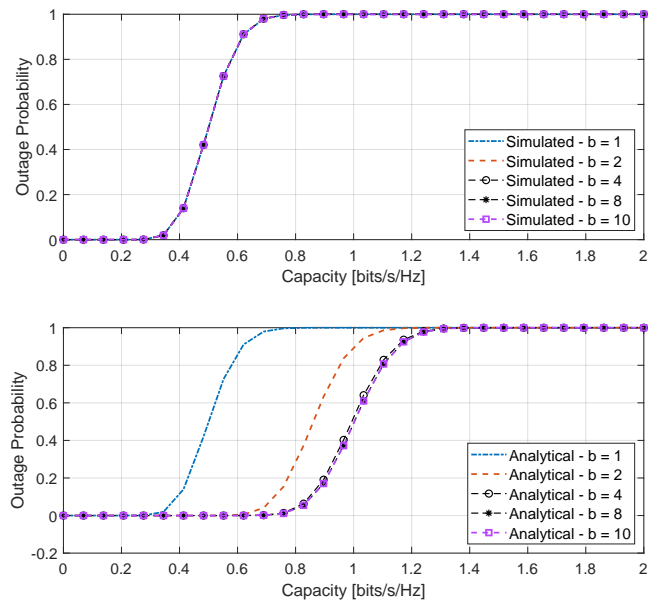


Figure 12. Outage probability for $N = 100$ and $b \in \{1, 2, 4, 8, 10\}$.

phase quantization.

V. CONCLUSION

In this paper, we have done an in-depth analysis of a practical LIS-assisted Single-Input Single-Output (SISO) system. Since quantization errors are unavoidable, we evaluate the influence of bits number dedicated to the phase quantization on spectral efficiency, symbol error rate, and outage probability. We compare such a system performance with the conventional one without LIS through accurate closed-form expressions derived for each of these metrics. We have extended our analysis to power scaling law and the power required to achieve specific

capacity. Not only is the influence of b verified, but also that of the number of LIS elements.

We can conclude that the performance improves as the number of LIS elements and bits increases. The LIS with approximately fifty elements and four dedicated bits for phase quantization outperforms the conventional system performance without LIS.

APPENDIX A

To find the parameters κ and θ for the approximated PDF of λ , we first need to define the following Lemmas.

Lemma 2.

$$\left| \sum_{n=1}^N z_n e^{j\theta_n} \right|^2 = \sum_{n=1}^N z_n^2 + 2 \sum_{m=1}^N \sum_{n=m+1}^N z_m z_n \cos(\theta_m - \theta_n). \quad (45)$$

Proof. This identity is straightforwardly found by expanding the summation terms on its left side. \square

Lemma 3. If $X \sim \mathcal{CN}(\mathbf{0}_M, \sigma_X^2 \mathbf{I}_M)$, then $Y = |X|$ is a Rayleigh random variable with PDF given by

$$f_Y(y) = \frac{2y}{\sigma_X^2} e^{-\frac{y^2}{\sigma_X^2}}, y \geq 0. \quad (46)$$

Proof. The proof for this Lemma is given in [30]. \square

Lemma 4. If Y is a Rayleigh random variable with PDF defined by (46), then, its 4 first moments are given by

$$\mathbb{E}[Y] = \int_0^\infty y f_Y(y) dy = \frac{\sigma_X \sqrt{\pi}}{2}, \quad (47)$$

$$\mathbb{E}[Y^2] = \int_0^\infty y^2 f_Y(y) dy = \sigma_X^2, \quad (48)$$

$$\mathbb{E}[Y^3] = \int_0^\infty y^3 f_Y(y) dy = \frac{3\sigma_X^3 \sqrt{\pi}}{4}, \quad (49)$$

$$\mathbb{E}[Y^4] = \int_0^\infty y^4 f_Y(y) dy = 2\sigma_X^4. \quad (50)$$

Lemma 5. If X is a uniform random variable with PDF given by

$$f_X(x) = \begin{cases} \frac{a}{2\pi}, & -\frac{\pi}{a} \leq x \leq \frac{\pi}{a}, \\ 0, & \text{otherwise,} \end{cases} \quad (51)$$

then $Y = -X$ has the same PDF as X , which was defined in (51).

Proof. This can be straightforwardly proved by noticing that the PDF of X is symmetrical around 0. \square

Lemma 6. If θ_m and θ_n are independent and identically distributed uniform random variables with PDF given by (51), then $Y = \theta_m + \theta_n$ has the following PDF

$$f_Y(y) = \begin{cases} \frac{a}{2\pi} \left(1 + \frac{a}{2\pi} y\right), & -\frac{2\pi}{a} \leq y \leq 0, \\ \frac{a}{2\pi} \left(1 - \frac{a}{2\pi} y\right), & 0 < y \leq \frac{2\pi}{a}, \\ 0, & \text{otherwise.} \end{cases} \quad (52)$$

Proof. From the theory, we know that the sum of two random variables equals the convolution of $f_{\theta_m}(\theta_m)$ and $f_{\theta_n}(\theta_n)$ is

$$f_Y(y) = \int_{-\infty}^{\infty} f_{\theta_m}(y - \theta_n) f_{\theta_n}(\theta_n) d\theta_n. \quad (53)$$

Therefore, $f_Y(y)$ is defined as

$$f_Y(y) = \begin{cases} \int_{-\frac{\pi}{a}+y}^{\frac{\pi}{a}+y} \frac{a^2}{4\pi^2} d\theta_n, & -\frac{2\pi}{a} \leq y < 0, \\ \int_{-\frac{\pi}{a}}^{\frac{\pi}{a}-y} \frac{a^2}{4\pi^2} d\theta_n, & 0 \leq y \leq \frac{2\pi}{a}, \\ 0, & \text{otherwise,} \end{cases} \quad (54)$$

which concludes the proof. \square

Lemma 7. If the PDF of the sum of two independent and identically distributed uniform random variables is given by (52), then

$$\mathbb{E}[\cos(\theta_m - \theta_n)] = \frac{a^2 \sin^2\left(\frac{\pi}{a}\right)}{\pi^2}. \quad (55)$$

Proof. By using Lemma 5, we can rewrite (55) as $\mathbb{E}[\cos(\theta_m + \theta_n)]$, then applying Lemma 6 we have

$$\begin{aligned} \mathbb{E}[\cos(\theta_m + \theta_n)] &= \mathbb{E}[\cos(y)] \\ &= \int_{-\frac{2\pi}{a}}^0 \cos(y) \frac{a}{2\pi} \left(1 + \frac{a}{2\pi} y\right) dy + \int_{-\frac{2\pi}{a}}^0 \cos(y) \frac{a}{2\pi} \left(1 - \frac{a}{2\pi} y\right) dy. \end{aligned} \quad (56)$$

Solving the two integrals in (56) concludes the proof. \square

Lemma 8. If the PDF of the sum of two independent and identically distributed uniform random variables is given by (52), then

$$\mathbb{E}[\cos^2(\theta_m - \theta_n)] = \frac{8\pi^2 + a^2 - a^2 \cos^2\left(\frac{4\pi}{a}\right)}{16\pi^2}. \quad (57)$$

Proof. By using Lemma 5 we can rewrite (55) as $\mathbb{E}[\cos^2(\theta_m + \theta_n)]$, then applying Lemma 6 we have

$$\begin{aligned} \mathbb{E}[\cos^2(\theta_m + \theta_n)] &= \mathbb{E}[\cos^2(y)] \\ &= \int_{-\frac{2\pi}{a}}^0 \cos^2(y) \frac{a}{2\pi} \left(1 + \frac{a}{2\pi} y\right) dy + \int_{-\frac{2\pi}{a}}^0 \cos^2(y) \frac{a}{2\pi} \left(1 - \frac{a}{2\pi} y\right) dy. \end{aligned} \quad (58)$$

Solving the two integrals in (58) concludes the proof. \square

Lemma 9. If X is a uniform random variable with PDF given by (51), then the PDF of $Y = 2X$ is given by

$$f_Y(y) = \frac{a}{4\pi}, -\frac{2\pi}{a} \leq y \leq \frac{2\pi}{a}. \quad (59)$$

Proof. This is proved by using the standard transformation of random variables. \square

Lemma 10. If θ_l , θ_m and θ_n are independent and identically distributed uniform random variables with PDF given by (51), then $Y = 2\theta_l - (\theta_m + \theta_n)$ has the following PDF

$$f_Y(y) = \begin{cases} \frac{a}{2\pi} + \frac{a^2 y}{4\pi^2} + \frac{a^3 y^2}{32\pi^3}, & -\frac{4\pi}{a} \leq y \leq -\frac{2\pi}{a}, \\ \frac{a}{4\pi} - \frac{a^3 y^2}{32\pi^3}, & -\frac{2\pi}{a} < y \leq 0, \\ \frac{a}{4\pi} - \frac{a^3 y^2}{32\pi^3}, & 0 < y \leq \frac{2\pi}{a}, \\ \frac{a}{2\pi} - \frac{a^2 y}{4\pi^2} + \frac{a^3 y^2}{32\pi^3}, & \frac{2\pi}{a} < y \leq \frac{4\pi}{a}, \\ 0, & \text{otherwise.} \end{cases} \quad (60)$$

Proof. We start by remembering that we know the PDF of $W = 2\theta_l$ and of $Z = \theta_m + \theta_n$, which are given by (59)

and (52), respectively. Next by applying Lemma 5, we can rewrite Y as $Y = Z + W$, which is the sum of two independent random variables. Therefore, the PDF of Y is the convolution between the PDFs of W and Z , which is defined as

$$f_Y(y) = \int_{-\infty}^{\infty} f_W(y-z)f_Z(z)dz. \quad (61)$$

Therefore, $f_Y(y)$ is defined as

$$f_Y(y) = \begin{cases} \int_{-\frac{2\pi}{a}+y}^{\frac{2\pi}{a}+y} \frac{a^2}{8\pi^2} \left(1 + \frac{a}{2\pi}z\right) dz, & -\frac{4\pi}{a} \leq y < -\frac{2\pi}{a}, \\ \int_0^{\frac{2\pi}{a}+y} \frac{a^2}{8\pi^2} \left(1 - \frac{a}{2\pi}z\right) dz + \int_{-\frac{\pi}{a}+y}^{\frac{\pi}{a}} \frac{a^2}{8\pi^2} \left(1 + \frac{a}{2\pi}z\right) dz, & -\frac{2\pi}{a} \leq y < 0, \\ \int_{-\frac{2\pi}{a}+y}^0 \frac{a^2}{8\pi^2} \left(1 + \frac{a}{2\pi}z\right) dz + \int_{-\frac{\pi}{a}+y}^{\frac{\pi}{a}} \frac{a^2}{8\pi^2} \left(1 - \frac{a}{2\pi}z\right) dz, & 0 \leq y < \frac{2\pi}{a}, \\ \int_{-\frac{2\pi}{a}+y}^{\frac{2\pi}{a}} \frac{a^2}{8\pi^2} \left(1 - \frac{a}{2\pi}z\right) dz, & \frac{2\pi}{a} \leq y \leq \frac{4\pi}{a}, \\ 0, & \text{otherwise,} \end{cases} \quad (62)$$

which concludes the proof. \square

Lemma 11. *If the PDF of the sum of three independent random variables, $Y = 2\theta_l - (\theta_m + \theta_n)$, is given by (60), then*

$$\mathbb{E}[\cos(2\theta_l - (\theta_m + \theta_n))] = \frac{a^3 \cos\left(\frac{\pi}{a}\right) \sin^3\left(\frac{\pi}{a}\right)}{\pi^3}. \quad (63)$$

Proof. By using Lemma 10 we have

$$\begin{aligned} \mathbb{E}[\cos(2\theta_l - (\theta_m + \theta_n))] &= \mathbb{E}[\cos(y)] \\ &= \int_{-\frac{4\pi}{a}}^{-\frac{2\pi}{a}} \cos(y) \left[\frac{a}{2\pi} + \frac{a^2 y}{4\pi^2} + \frac{a^3 y^2}{32\pi^3} \right] dy \\ &\quad + \int_{-\frac{2\pi}{a}}^{\frac{2\pi}{a}} \cos(y) \left[\frac{a}{4\pi} - \frac{a^3 y^2}{32\pi^3} \right] dy \\ &\quad + \int_{\frac{2\pi}{a}}^{\frac{4\pi}{a}} \cos(y) \left[\frac{a}{2\pi} - \frac{a^2 y}{4\pi^2} + \frac{a^3 y^2}{32\pi^3} \right] dy. \end{aligned} \quad (64)$$

Solving the three integrals in (64) concludes the proof. \square

Lemma 12. *If θ_l , θ_m , and θ_n are independent and identically distributed uniform random variables with PDF given by (51), then*

$$\mathbb{E}[\cos(\theta_l - \theta_m) \cos(\theta_l - \theta_n)] = \frac{a^2 \sin^2\left(\frac{\pi}{a}\right) [2\pi + a \sin\left(\frac{2\pi}{a}\right)]}{4\pi^3}. \quad (65)$$

Proof. We start by applying the trigonometric identity $\cos(a) \cos(b) = \frac{\cos(a-b) + \cos(a+b)}{2}$ to (66), which then can be re-written as

$$\begin{aligned} \mathbb{E}[\cos(\theta_l - \theta_m) \cos(\theta_l - \theta_n)] &= \frac{1}{2} \mathbb{E}[\cos(\theta_n - \theta_m)] \\ &\quad + \frac{1}{2} \mathbb{E}[\cos(2\theta_l - \theta_n - \theta_m)]. \end{aligned} \quad (66)$$

Next, by applying Lemmas 7 and 11 to (66), we conclude the proof. \square

A. Approximated PDF of the Instantaneous SNR

Let the random variable $Z = r$, where r is defined in (6), therefore, the PDF of Z can be accurately approximated by a Gamma distribution with parameters κ and θ , defined by (7) and (8), respectively. This is empirically proven by comparing the normalized histogram of Z against the theoretical PDF of a Gamma random variable, Y , with the parameters defined earlier.

In order to approximate Z as a Gamma random variable, Y , we have to find the parameters shape and scale (*i.e.*, κ and θ) based on statistical information of Z . Therefore, we approximate Z as a Gamma random variable, Y , by using two different moments of Y and then assuming that $\mathbb{E}[Y^2] = \mathbb{E}[Z^2]$ and $\mathbb{E}[Y^4] = \mathbb{E}[Z^4]$.

Those two moments of the Gamma distribution Y are defined as

$$\mathbb{E}[Y^2] = \kappa(\kappa + 1)\theta^2, \quad (67)$$

and

$$\mathbb{E}[Y^4] = \kappa(\kappa + 1)(\kappa + 2)(\kappa + 3)\theta^4. \quad (68)$$

Based on (67), the assumption that $\mathbb{E}[Y^2] = \mathbb{E}[Z^2]$ and then isolating θ we find

$$\theta = \sqrt{\frac{\mathbb{E}[Z^2]}{\kappa(\kappa + 1)}}. \quad (69)$$

Next, plugging (69) back into (68) and assuming that $\mathbb{E}[Y^4] = \mathbb{E}[Z^4]$, we find κ as

$$\left(\mathbb{E}[Z^4] - \mathbb{E}[Z^2]^2\right) \kappa^2 + \left(\mathbb{E}[Z^4] - 5\mathbb{E}[Z^2]^2\right) \kappa - 6\mathbb{E}[Z^2]^2 = 0, \quad (70)$$

which is a quadratic equation with the following two roots

$$\begin{aligned} \kappa_0 &= \frac{-\left(\mathbb{E}[Z^4] - 5\mathbb{E}[Z^2]^2\right) + \sqrt{\mathbb{E}[Z^4]^2 - 34\mathbb{E}[Z^4]\mathbb{E}[Z^2]^2 + 49\mathbb{E}[Z^2]^4}}{2\left(\mathbb{E}[Z^4] - \mathbb{E}[Z^2]^2\right)}, \\ \kappa_1 &= \frac{-\left(\mathbb{E}[Z^4] - 5\mathbb{E}[Z^2]^2\right) - \sqrt{\mathbb{E}[Z^4]^2 - 34\mathbb{E}[Z^4]\mathbb{E}[Z^2]^2 + 49\mathbb{E}[Z^2]^4}}{2\left(\mathbb{E}[Z^4] - \mathbb{E}[Z^2]^2\right)}, \end{aligned} \quad (72)$$

where out of the two roots, only is useful, *i.e.*, only one root has a positive value. Since κ ought to be a real and positive number, we assume that the value within the square root is a positive one. Next, assuming that $5\mathbb{E}[Z^2]^2 \geq \mathbb{E}[Z^4]$, then only κ_0 results in a positive value.

Next, in order to find the moment $\mathbb{E}[Z^2]$, we first expand $\mathbb{E}[Z^2]$ as

$$\begin{aligned} \mathbb{E}[Z^2] &= \mathbb{E}[\gamma] \\ &= \mathbb{E}\left[\rho \left| \sum_{n=1}^N |h_n| |g_n| e^{j\delta_n} \right|^2\right] \\ &= \mathbb{E}\left[\rho \sum_{n=1}^N d_n^2 + 2\rho \sum_{m=1}^N \sum_{n=m+1}^N d_m d_n \cos(\delta_m - \delta_n)\right], \end{aligned} \quad (73)$$

where $d_k = |h_k| |g_k|$ and the last line is found by applying Lemma 2. Thus, using the fact that $|h_n|$, $|g_n|$, and δ_n , $\forall n$ are mutually independent random variables and that h_m and h_n ,

and g_m and g_n , $\forall m, n$ are identically distributed, then (73), can be re-written as

$$\begin{aligned} \mathbb{E}[Z^2] &= \rho \sum_{n=1}^N \mathbb{E}[|h_n|^2] \mathbb{E}[|g_n|^2] \\ &+ 2\rho \sum_{m=1}^N \sum_{n=m+1}^N \mathbb{E}[|h_m|^2] \mathbb{E}[|g_m|^2] \mathbb{E}[\cos(\delta_m - \delta_n)]. \end{aligned} \quad (74)$$

Then, by applying Lemmas 4 and 7 to (74), we find (11).

Next, in order to find the moment $\mathbb{E}[Z^4]$, we initially expand it as

$$\begin{aligned} \mathbb{E}[Z^4] &= \mathbb{E}[\gamma^2] \\ &= \mathbb{E}\left[\left(\sum_{l=1}^N d_l^2\right)^2\right] \\ &+ 4 \sum_{l=1}^N \sum_{m=1}^N \sum_{n=m+1}^N \mathbb{E}[d_l^2 d_m d_n \cos(\delta_m - \delta_n)] \\ &+ 4\mathbb{E}\left[\left(\sum_{m=1}^N \sum_{n=m+1}^N d_m d_n \cos(\delta_m - \delta_n)\right)^2\right], \end{aligned} \quad (75)$$

where $d_k = |h_k||g_k|$. The first term of (75) can be expressed as

$$\begin{aligned} \mathbb{E}\left[\left(\sum_{l=1}^N d_l^2\right)^2\right] &= \mathbb{E}\left[\sum_{n=1}^N d_n^4 + \sum_{m=1}^N \sum_{n=1, n \neq m}^N d_m^2 d_n^2\right] \\ &= N\mathbb{E}[|g_m|^4] \mathbb{E}[|h_m|^4] \\ &+ N(N-1)\mathbb{E}[|g_m|^2]^2 \mathbb{E}[|h_m|^2]^2 \\ &= N(N+3)(\beta_g \beta_h)^2, \end{aligned} \quad (76)$$

where the last line of (76) is found by applying Lemma 4. Next, the second term of (75) can be expressed as (77), where the last line is found by applying Lemmas 4 and 7. Then, the third term of (75) can be expressed as (78), where the last line is found after applying Lemmas 4, 7, 8, and 12. Finally, after plugging (76), (77), and (78) back into (75) and several simplifications, we find (12).

The proof is concluded by replacing Equations (11) and (12) into the definitions of κ and θ , given by (71) and (69), respectively.

APPENDIX B

For the derivation of Remark 1, we need to define the following Lemma.

Lemma 13.

$$\lim_{x \rightarrow 0} \frac{\sin(x)}{x} = 1. \quad (79)$$

Proof. We prove Lemma 13 by applying L'Hôpital's rule to (79) as shown next

$$\lim_{x \rightarrow 0} \frac{\frac{\partial \sin(x)}{\partial x}}{\frac{\partial x}{\partial x}} = \lim_{x \rightarrow 0} \cos(x) = 1. \quad (80)$$

Lemma 14.

$$\lim_{x \rightarrow \infty} \left(x \sin\left(\frac{a}{x}\right)\right)^n = a^n, \forall a, n \in \mathbb{R}. \quad (81)$$

Proof. We start by re-writing (81) as

$$\left(\lim_{x \rightarrow \infty} a \frac{\sin\left(\frac{a}{x}\right)}{\frac{1}{x}}\right)^n = \left(\lim_{x \rightarrow \infty} a \frac{\sin\left(\frac{a}{x}\right)}{\frac{a}{x}}\right)^n, \quad (82)$$

where we also used the power rule of limits to re-write it. Next, we apply the following change of variables $\theta = \frac{a}{x}$ to (82), resulting in

$$\left(\lim_{\theta \rightarrow 0} a \frac{\sin(\theta)}{\theta}\right)^n = a^n \left(\lim_{\theta \rightarrow 0} \frac{\sin(\theta)}{\theta}\right)^n, \quad (83)$$

where we used the constant multiple rule of limits to find the last part. Next, by using Lemma 13, we conclude the proof. \square

A. Derivation of Remark 1

The results (13) and (14) are found after expanding (11) and (12), using Lemma 14 and the fact that $\lim_{x \rightarrow \infty} \cos(1/x) = 1$.

APPENDIX C

For the proof of (17) we should notice that when $\lim_{\rho \rightarrow \infty} \theta = \infty$ then, consequently, $\lim_{\rho \rightarrow \infty} -\frac{1}{4\theta^2} = 0$. Therefore,

$$\lim_{\rho \rightarrow \infty} {}_2F_3\left(1, 1; 2, \frac{3}{2} - \frac{\kappa}{2}, 2 - \frac{\kappa}{2}; -\frac{1}{4\theta^2}\right) = 1. \quad (84)$$

$$\lim_{\rho \rightarrow \infty} {}_1F_2\left(\frac{\kappa}{2} + \frac{1}{2}; \frac{3}{2}, \frac{\kappa}{2} + \frac{3}{2}; -\frac{1}{4\theta^2}\right) = 1. \quad (85)$$

$$\lim_{\rho \rightarrow \infty} {}_1F_2\left(\frac{\kappa}{2}; \frac{1}{2}, \frac{\kappa}{2} + 1; -\frac{1}{4\theta^2}\right) = 1. \quad (86)$$

Hence, in high SNR regime (16) can be tightly approximated as (17), which concludes the proof.

APPENDIX D

The proof of (18) is straightforwardly found by noticing that the first three terms of (17) tend to 0 when $\rho \rightarrow \infty$, since $\theta \rightarrow \infty$ when $\rho \rightarrow \infty$, which concludes this proof.

APPENDIX E

In high SNR regime, as $N \rightarrow \infty$ and $\kappa \rightarrow \infty$, $\Gamma(\kappa)$ grows even faster. Therefore,

$$\lim_{N \rightarrow \infty} \frac{2\pi \sec\left(\frac{\pi\kappa}{2}\right)}{(\kappa+1)\theta^{\kappa+1}\Gamma(\kappa)\log(4)} = 0. \quad (87)$$

$$\lim_{N \rightarrow \infty} \frac{2\pi \csc\left(\frac{\pi\kappa}{2}\right)}{\kappa\theta^\kappa\Gamma(\kappa)\log(4)} = 0. \quad (88)$$

These two terms tend to 0 faster than the other 2 terms, concluding the proof. \square

$$\begin{aligned}
4 \sum_{l=1}^N \sum_{m=1}^N \sum_{n=m+1}^N \mathbb{E} [d_l^2 d_m d_n \cos(\delta_m - \delta_n)] &= 4 \sum_{m=1}^N \sum_{n=1, n \neq m}^N \mathbb{E} [d_m^3 d_n \cos(\delta_m - \delta_n)] \\
&+ 4 \sum_{l=1}^N \sum_{m=1, m \neq l}^N \sum_{n=m+1, n \neq l}^N \mathbb{E} [d_l^2 d_m d_n \cos(\delta_m - \delta_n)] \\
&= 4N(N-1) \mathbb{E} [|g_m|^3] \mathbb{E} [|h_m|^3] \mathbb{E} [|g_m|] \mathbb{E} [|h_m|] \mathbb{E} [\cos(\delta_l - \delta_m)] \\
&+ 2N(N-1)(N-2) \mathbb{E} [|g_l|^2] \mathbb{E} [|h_l|^2] \mathbb{E} [|g_m|] \mathbb{E} [|h_m|] \mathbb{E} [|g_n|] \mathbb{E} [|h_n|] \cos(\delta_m - \delta_n) \\
&= \frac{1}{16} N(N-1)(2N+5) (\beta_g \beta_h)^2 Q^2 \sin^2 \left(\frac{\pi}{Q} \right). \tag{77}
\end{aligned}$$

$$\begin{aligned}
4\mathbb{E} \left[\left(\sum_{m=1}^N \sum_{n=m+1}^N d_m d_n \cos(\delta_m - \delta_n) \right)^2 \right] &= 4 \sum_{j=1}^N \sum_{l=j+1}^N \sum_{m=1}^N \sum_{n=m+1}^N \mathbb{E} [d_j d_l d_m d_n \cos(\delta_j - \delta_l) \cos(\delta_m - \delta_n)] \\
&= 4 \sum_{j=1}^N \sum_{l=j+1}^N \sum_{m=1, m=j}^N \sum_{n=m+1, n=l}^N \mathbb{E} [d_j^2 d_l^2 \cos^2(\delta_j - \delta_l)] \\
&+ 8 \sum_{l=1}^N \sum_{m=1, m \neq l}^N \sum_{n=m+1, n \neq l}^N \mathbb{E} [d_l^2 d_m d_n \cos(\delta_l - \delta_m) \cos(\delta_l - \delta_n)] \\
&+ 4 \sum_{j=1}^N \sum_{l=1, l \neq j}^N \sum_{m=1, m \neq j}^N \sum_{n=1, n \neq j}^N \mathbb{E} [d_j d_l d_m d_n \cos(\delta_j - \delta_l) \cos(\delta_m - \delta_n)] \\
&= \frac{N(N-1) (\beta_g \beta_h)^2 \left\{ Q^2 \left[\pi(N-2) \sin^2 \left(\frac{\pi}{Q} \right) \left(\pi \left((N-3) Q^2 \sin^2 \left(\frac{\pi}{Q} \right) + 32 \right) + 16Q \sin \left(\frac{2\pi}{Q} \right) - 32 \cos \left(\frac{4\pi}{Q} \right) \right] + 32(Q^2 + 8\pi^2) \right\}}{256\pi^2}. \tag{78}
\end{aligned}$$

APPENDIX F

Here we outline the derivation of C_{lower} in (24). We start by applying the Taylor series expansion of $1/\gamma$ around $\mathbb{E}[\gamma]$ [21], the term $\mathbb{E}[1/\gamma]$ in (27) can be approximated as [31]

$$\mathbb{E} \left[\frac{1}{\gamma} \right] \approx \frac{1}{\mathbb{E}[\gamma]} + \frac{\text{var}(\gamma)}{\mathbb{E}[\gamma]^3} = \frac{\mathbb{E}[\gamma^2]}{\mathbb{E}[\gamma]^3}. \tag{89}$$

After replacing $\mathbb{E}[\gamma]$ and $\mathbb{E}[\gamma^2]$ in (89) via (11) and (12), respectively, and then by substituting the resultant expression into (27), C_{lower} can be approximated as shown in the second part of (24).

APPENDIX G

Here we describe the derivation of the outage probability given by (34). Using the PDF of the instantaneous capacity given by (20), the outage probability can be written as

$$\begin{aligned}
P_{\text{out.}} &= \Pr\{C_{\text{inst.}} < C_{\text{out.}}\} \\
&= \frac{\log(2)}{\Gamma(\kappa)\theta^\kappa} \int_0^{C_{\text{out.}}} 2^{u-1} (2^u - 1)^{\left(\frac{\kappa-2}{2}\right)} e^{-\frac{\sqrt{2^u-1}}{\theta}} du. \tag{90}
\end{aligned}$$

Next, using the following change of variable $x = 2^u - 1$, then (90) becomes

$$P_{\text{out.}} = \frac{1}{2\Gamma(\kappa)\theta^\kappa} \int_0^{2^{C_{\text{out.}}}-1} x^{\left(\frac{\kappa-2}{2}\right)} e^{-\frac{\sqrt{x}}{\theta}} dx. \tag{91}$$

Finally, using (2.33.10) from [21]

$$\int x^m e^{-\beta x^n} dx = -\frac{\Gamma\left(\frac{m+1}{n}, \beta x^n\right)}{n\beta^{\frac{m+1}{n}}}, \tag{92}$$

we find a solution for the the integral in (91), which concludes the proof.

APPENDIX H

For the proofs of (36) and (37), we first to define the following Lemmas.

Lemma 15. According to (Eq. 8.2.5, [23])

$$1 - \frac{\Gamma(a, b)}{\Gamma(a)} = \frac{\gamma(a, b)}{\Gamma(a)}, \tag{93}$$

where $\gamma(a, b)$ is the lower incomplete gamma function.

Lemma 16. According to (Eq. 8.5.1, [23])

$$\gamma(a, b) = a^{-1} b^a {}_1F_1(a, a+1, -b). \tag{94}$$

Lemma 17. According to (07.20.03.0001.01) of [32]

$${}_1F_1(a, b, 0) = 1. \tag{95}$$

Therefore, applying Lemmas 15 and 16, defined above, to (35) we end up with (36), which concludes the proof. Now, (37) is found by applying Lemma 17 to (36) and remembering that $\lim_{\rho \rightarrow \infty} \theta = \infty$, then $\lim_{\rho \rightarrow \infty} 1/\theta = 0$.

APPENDIX I

In this Appendix, we derive the average symbol error rate expression given by (40), but first, we need to establish some Lemmas.

Lemma 18.

$$\mathcal{Q}(x) = \frac{1}{2} \left[1 - \text{erf} \left(\frac{x}{\sqrt{2}} \right) \right]. \tag{96}$$

This relation is given by (Eq. B.111, [33]).

Lemma 19.

$$\int_0^\infty x^m e^{-\beta x^n} dx = \frac{\Gamma\left(\frac{m+1}{n}\right)}{n\beta^{\frac{m+1}{n}}}. \tag{97}$$

This relation is given by (Eq. 3.326.2, [21]).

Lemma 20. If $\text{erf}(\cdot)$ is the Gauss error function, and a, b , and $c > 0$, then the integral $\int_0^\infty \text{erf}(ax) x^b e^{-cx} dx$ is given by (98). The integral in (98) is found by using an integral solver [34].

$$\begin{aligned} \int_0^\infty \text{erf}(ax) x^b e^{-cx} dx &= c^{-b-1} \Gamma(b+1) \\ &+ \frac{ca^{-b-2} \Gamma\left(\frac{b+3}{2}\right) {}_2F_2\left(\frac{b}{2}+1, \frac{b}{2}+\frac{3}{2}; \frac{3}{2}, \frac{b}{2}+2; \frac{c^2}{4a^2}\right)}{\sqrt{\pi}(b+2)} \\ &- \frac{a^{-b-1} \Gamma\left(\frac{b}{2}+1\right) {}_2F_2\left(\frac{b}{2}+\frac{1}{2}, \frac{b}{2}+1; \frac{1}{2}, \frac{b}{2}+\frac{3}{2}; \frac{c^2}{4a^2}\right)}{\sqrt{\pi}(b+1)}. \end{aligned} \quad (98)$$

A. Proof of the Average Symbol Error Rate

By using the fact that $\gamma = r^2$ (see (6)), the expectation of the conditional symbol error probability given the distribution of the SNR can be written as

$$\begin{aligned} P_e &= \mathbb{E} \left[a\mathcal{Q}\left(\sqrt{b\gamma}\right) \right] = \mathbb{E} \left[a\mathcal{Q}\left(\sqrt{br}\right) \right] \\ &= \int_0^\infty P_{e|\gamma}(x) f_R(x) dx, \end{aligned} \quad (99)$$

where $f_R(r)$ is the PDF of the Gamma distribution, which tightly approximates the exact PDF of the random variable, r .

By plugging $P_{e|\gamma} = a\mathcal{Q}(\sqrt{b\gamma})$ and the Gamma PDF back into (99), the average SER is rewritten as

$$P_e = \frac{a}{\Gamma(\kappa)\theta^\kappa} \int_0^\infty \mathcal{Q}\left(\sqrt{bx}\right) x^{\kappa-1} e^{-x/\theta} dx. \quad (100)$$

By using Lemma 18, (100) can be equivalently rewritten as

$$\begin{aligned} P_e &= \frac{a}{\Gamma(\kappa)\theta^\kappa} \left[\int_0^\infty x^{\kappa-1} e^{-x/\theta} dx \right. \\ &\quad \left. - \int_0^\infty \text{erf}\left(\sqrt{\frac{b}{2}x}\right) x^{\kappa-1} e^{-x/\theta} dx \right]. \end{aligned} \quad (101)$$

The first integral inside the square brackets of (101) is found by applying Lemma 19 to it, which results in

$$\int_0^\infty x^{\kappa-1} e^{-x/\theta} dx = \Gamma(\kappa)\theta^\kappa. \quad (102)$$

The second integral inside the square brackets of (101) is found by applying Lemma 20 to it, which results in

$$\begin{aligned} \int_0^\infty \text{erf}\left(\sqrt{\frac{b}{2}x}\right) x^{\kappa-1} e^{-x/\theta} dx \\ = \theta^\kappa \Gamma(\kappa) - \frac{2^{\kappa/2} b^{-\frac{\kappa}{2}} \Gamma\left(\frac{\kappa+1}{2}\right) {}_2F_2\left(\frac{\kappa}{2}+\frac{1}{2}, \frac{\kappa}{2}; \frac{1}{2}, \frac{\kappa}{2}+1; \frac{1}{2b\theta^2}\right)}{\sqrt{\pi}\kappa} \\ + \frac{2^{\frac{\kappa}{2}+\frac{1}{2}} b^{-\frac{\kappa}{2}-\frac{1}{2}} \Gamma\left(\frac{\kappa}{2}+1\right) {}_2F_2\left(\frac{\kappa}{2}+\frac{1}{2}, \frac{\kappa}{2}+1; \frac{3}{2}, \frac{\kappa}{2}+\frac{3}{2}; \frac{1}{2b\theta^2}\right)}{\sqrt{\pi}\theta(\kappa+1)}. \end{aligned} \quad (103)$$

Finally, by substituting (102) and (103) back into (101), we conclude the proof.

APPENDIX J

For the proof of (39) we should notice that when $\lim_{\rho \rightarrow \infty} \theta = \infty$ then, consequently, $\lim_{\rho \rightarrow \infty} \frac{1}{2\theta^2} = 0$. Therefore,

$$\lim_{\rho \rightarrow \infty} {}_2F_2\left(\frac{\kappa}{2}+\frac{1}{2}, \frac{\kappa}{2}; \frac{1}{2}, \frac{\kappa}{2}+1; \frac{1}{2b\theta^2}\right) = 1. \quad (104)$$

$$\lim_{\rho \rightarrow \infty} {}_2F_2\left(\frac{\kappa}{2}+\frac{1}{2}, \frac{\kappa}{2}+1; \frac{3}{2}, \frac{\kappa}{2}+\frac{3}{2}; \frac{1}{2b\theta^2}\right) = 1. \quad (105)$$

Hence, in high SNR regime (40) can be tightly approximated as (39), which concludes the proof.

APPENDIX K

In order to derive the diversity order, we first need to rewrite (11) and (12) as

$$\mathbb{E}[\gamma] = \rho\beta_g\beta_h\mathcal{A}_1, \quad (106)$$

and

$$\mathbb{E}[\gamma^2] = (\rho\beta_g\beta_h)^2 \mathcal{A}_2, \quad (107)$$

respectively, where \mathcal{A}_1 and \mathcal{A}_2 do not depend on the average SNR, ρ . By plugging these two equation back into (7) and (8), we find

$$\kappa = \frac{5\mathcal{A}_1^2 + \sqrt{49\mathcal{A}_1^4 - 34\mathcal{A}_1^2\mathcal{A}_2 + \mathcal{A}_2^2} - \mathcal{A}_2}{2(\mathcal{A}_2 - \mathcal{A}_1^2)} > 0, \quad (108)$$

which also does not depend on the average SNR, and

$$\begin{aligned} \theta &= \rho^{\frac{1}{2}} \sqrt{\frac{\beta_g\beta_h \left(2\mathcal{A}_1^2 - \sqrt{\mathcal{A}_1^4 + 14\mathcal{A}_1^2\mathcal{A}_2 + \mathcal{A}_2^2} + 2\mathcal{A}_2\right)}{6\mathcal{A}_1}} \\ &= \rho^{\frac{1}{2}} \theta' > 0, \end{aligned} \quad (109)$$

which depends on the average SNR. Therefore, in high-SNR regime, (39) can be written as

$$P_e^{\text{high-SNR}} \approx \mathcal{B}_1 \rho^{-\frac{\kappa}{2}} - \mathcal{B}_2 \rho^{-\frac{(\kappa+1)}{2}}, \quad (110)$$

where

$$\mathcal{B}_1 = \frac{a2^{-\frac{(\kappa+2)}{2}} b^{-\frac{\kappa}{2}} \theta'^{-\kappa}}{\Gamma\left(\frac{\kappa}{2}+1\right)}, \quad (111)$$

and

$$\mathcal{B}_2 = \frac{\kappa a 2^{-\frac{(\kappa+3)}{2}} b^{-\frac{(\kappa+1)}{2}} \theta'^{-(\kappa+1)}}{\Gamma\left(\frac{\kappa+3}{2}\right)}. \quad (112)$$

Note that \mathcal{B}_1 and \mathcal{B}_2 do not depend on the average SNR, *i.e.*, they are independent from it. Furthermore, from (110), we realise that the terms $\rho^{-\frac{\kappa}{2}}$ and $\rho^{-\frac{(\kappa+1)}{2}}$ contribute with diversity order of $\frac{\kappa}{2}$ and $\frac{(\kappa+1)}{2}$, respectively. Therefore, the diversity order is calculated as

$$D = \min\left(\frac{\kappa}{2}, \frac{(\kappa+1)}{2}\right). \quad (113)$$

Since $\kappa > 0$, then (113) is simplified as

$$D = \frac{\kappa}{2}. \quad (114)$$

The proof is concluded after plugging (108) into (114).

REFERENCES

- [1] W. Hou, T. Fujino, and T. Kojima, "Quantization error reduction for MIMO detection based on orthogonal lattices," in *IEICE Communications Express*, vol. 2, pp. 42–48, 2013.
- [2] K. Kotera, O. Muta, and H. Furukawa, "Efficient nonlinear equalization scheme for MIMO constant envelope modulation receivers affected by quantization error," in *The International Conference on Information Network 2012*, pp. 275–279, 2012.
- [3] Özgecan Özdoğan, E. Björnson, and E. G. Larsson, "Intelligent reflecting surfaces: Physics, propagation, and pathloss modeling," 2019.
- [4] Q. Wu and R. Zhang, "Intelligent reflecting surface enhanced wireless network via joint active and passive beamforming," *IEEE Transactions on Wireless Communications*, vol. 18, no. 11, pp. 5394–5409, 2019.
- [5] H. Han, J. Zhao, D. Niyato, M. D. Renzo, and Q. Pham, "Intelligent reflecting surface aided network: Power control for physical-layer broadcasting," in *IEEE International Conference on Communications (ICC)*, pp. 1–7, 2020.
- [6] J. Ye, S. Guo, and M. Alouini, "Joint reflecting and precoding designs for ser minimization in reconfigurable intelligent surfaces assisted mimo systems," *IEEE Transactions on Wireless Communications*, vol. 19, no. 8, pp. 5561–5574, 2020.
- [7] M.-A. Badiu and J. P. Coon, "Communication Through a Large Reflecting Surface With Phase Errors," *arXiv e-prints*, p. arXiv:1906.10751, Jun. 2019.
- [8] S. Abeywickrama, R. Zhang, and C. Yuen, "Intelligent reflecting surface: Practical phase shift model and beamforming optimization," in *IEEE International Conference on Communications (ICC)*, pp. 1–6, 2020.
- [9] Y. Han, W. Tang, S. Jin, C. Wen, and X. Ma, "Large intelligent surface-assisted wireless communication exploiting statistical CSI," *IEEE Transactions on Vehicular Technology*, vol. 68, no. 8, pp. 8238–8242, 2019.
- [10] R. C. Ferreira, M. S. P. Facina, F. A. P. De Figueiredo, G. Fraidenraich, and E. R. De Lima, "Bit error probability for large intelligent surfaces under double-nakagami fading channels," *IEEE Open Journal of the Communications Society*, vol. 1, pp. 750–759, 2020.
- [11] D. Gesbert, H. Bolcskei, D. A. Gore, and A. J. Paulraj, "Outdoor MIMO wireless channels: models and performance prediction," *IEEE Transactions on Communications*, vol. 50, no. 12, pp. 1926–1934, 2002.
- [12] Y. Ai, M. Cheffena, A. Mathur, and H. Lei, "On physical layer security of double Rayleigh fading channels for vehicular communications," *IEEE Wireless Communications Letters*, vol. 7, no. 6, pp. 1038–1041, 2018.
- [13] J. Salo, H. M. El-Sallabi, and P. Vainikainen, "Impact of double-Rayleigh fading on system performance," in *International Symposium on Wireless Pervasive Computing*, p. 5, 2006.
- [14] H. Shin and M. Z. Win, "MIMO diversity in the presence of double scattering," *IEEE Transactions on Information Theory*, vol. 54, no. 7, pp. 2976–2996, 2008.
- [15] T. Wang, G. Chen, J. P. Coon, and M.-A. Badiu, "Study of intelligent reflective surface assisted communications with one-bit phase adjustments," 2020.
- [16] T. L. Marzetta, *Fundamentals of massive MIMO*. Cambridge University Press, 2016.
- [17] M. D. Renzo, F. H. Danufane, X. Xi, J. de Rosny, and S. Tretyakov, "Analytical modeling of the path-loss for reconfigurable intelligent surfaces – anomalous mirror or scatterer?," 2020.
- [18] Q. Wu and R. Zhang, "Beamforming optimization for intelligent reflecting surface with discrete phase shifts," in *IEEE International Conference on Acoustics, Speech and Signal Processing (ICASSP)*, pp. 7830–7833, May 2019.
- [19] E. Basar, M. Di Renzo, J. De Rosny, M. Debbah, M.-S. Alouini, and R. Zhang, "Wireless communications through reconfigurable intelligent surfaces," *IEEE Access*, vol. 7, p. 116753–116773, 2019.
- [20] E. Basar, "Transmission through large intelligent surfaces: A new frontier in wireless communications," in *European Conference on Networks and Communications (EuCNC)*, pp. 112–117, Jun. 2019.
- [21] I. S. Gradshteyn and I. M. Ryzhik. 7th ed.
- [22] Wolfram Research, "Mathematica," 2018.
- [23] "NIST Digital Library of Mathematical Functions." <http://dlmf.nist.gov/>, Release 1.0.25 of 2019-12-15. F. W. J. Olver, A. B. Olde Daalhuis, D. W. Lozier, B. I. Schneider, R. F. Boisvert, C. W. Clark, B. R. Miller, B. V. Saunders, H. S. Cohl, and M. A. McClain, eds.
- [24] M. Abramowitz and I. A. Stegun, *Handbook of Mathematical Functions with Formulas, Graphs, and Mathematical Tables*. New York: Dover, ninth dover printing, tenth GPO printing ed., 1964.
- [25] J. Proakis and M. Salehi, *Digital Communications*. McGraw-Hill, 2008.
- [26] Zhengdao Wang and G. B. Giannakis, "A simple and general parameterization quantifying performance in fading channels," *IEEE Transactions on Communications*, vol. 51, no. 8, pp. 1389–1398, 2003.
- [27] F. A. Pereira de Figueiredo, C. F. Dias, E. Rodrigues de Lima, and G. Fraidenraich, "Capacity bounds for dense massive MIMO in a line-of-sight propagation environment," Dec. 2019.
- [28] F. A. P. De Figueiredo, F. A. C. M. Cardoso, I. Moerman, and G. Fraidenraich, "On the application of massive MIMO systems to machine type communications," *IEEE Access*, vol. 7, pp. 2589–2611, 2019.
- [29] S. Kullback and R. A. Leibler, "On information and sufficiency," *Ann. Math. Statist.*, vol. 22, pp. 79–86, Mar. 1951.
- [30] A. Papoulis and S. U. Pillai, *Probability, Random Variables, and Stochastic Processes*. Boston: McGraw Hill, 4th ed., 2002.
- [31] Q. Zhang, S. Jin, K. Wong, H. Zhu, and M. Matthaiou, "Power scaling of uplink massive MIMO systems with arbitrary-rank channel means," *IEEE Journal of Selected Topics in Signal Processing*, vol. 8, no. 5, pp. 966–981, 2014.
- [32] Wolfram Research, "The wolfram functions site," Oct. 2001.
- [33] J. Shynk, *Probability, Random Variables, and Random Processes: Theory and Signal Processing Applications*. Wiley, 2012.
- [34] W. R. Inc., "Mathematica, Version 12.1." Champaign, IL, 2020.